

# DeepBeam: Deep Waveform Learning for Coordination-Free Beam Management in mmWave Networks

Michele Polese, Francesco Restuccia, and Tommaso Melodia

Institute for the Wireless Internet of Things, Northeastern University, Boston, MA, United States

## ABSTRACT

Highly directional millimeter wave (mmWave) radios need to perform *beam management* to establish and maintain reliable links. To achieve this objective, existing solutions mostly rely on explicit coordination between the transmitter (TX) and the receiver (RX), which significantly reduces the airtime available for communication and further complicates the network protocol design. This paper advances the state of the art by presenting *DeepBeam*, a framework for beam management that does not require pilot sequences from the TX, nor any beam sweeping or synchronization from the RX. This is achieved by inferring (i) the Angle of Arrival (AoA) of the beam and (ii) the actual beam being used by the transmitter through *waveform-level deep learning* on *ongoing transmissions* between the TX to other receivers. In this way, the RX can associate Signal-to-Noise-Ratio (SNR) levels to beams without explicit coordination with the TX. This is possible because different beam patterns introduce different “impairments” to the waveform, which can be subsequently learned by a convolutional neural network (CNN). To demonstrate the generality of DeepBeam, we conduct an extensive experimental data collection campaign where we collect more than 4 TB of mmWave waveforms with (i) 4 phased array antennas at 60.48 GHz, (ii) 2 codebooks containing 24 one-dimensional beams and 12 two-dimensional beams; (iii) 3 receiver gains; (iv) 3 different AoAs; (v) multiple TX and RX locations. Moreover, we collect waveform data with two custom-designed mmWave software-defined radios with fully-digital beamforming architectures at 58 GHz. We also implement our learning models in FPGA to evaluate latency performance. Results show that *DeepBeam* (i) achieves accuracy of up to 96%, 84% and 77% with a 5-beam, 12-beam and 24-beam codebook, respectively; (ii) reduces latency by up to 7x with respect to the 5G NR initial beam sweep in a default configuration and with a 12-beam codebook. The waveform dataset and the full *DeepBeam* code repository are publicly available.

## CCS CONCEPTS

• **Networks** → **Mobile networks**; *Link-layer protocols*.

### ACM Reference Format:

Michele Polese, Francesco Restuccia, and Tommaso Melodia. 2021. *DeepBeam: Deep Waveform Learning for Coordination-Free Beam Management in mmWave Networks*. In *The Twenty-second International Symposium on*

Permission to make digital or hard copies of all or part of this work for personal or classroom use is granted without fee provided that copies are not made or distributed for profit or commercial advantage and that copies bear this notice and the full citation on the first page. Copyrights for components of this work owned by others than the author(s) must be honored. Abstracting with credit is permitted. To copy otherwise, or republish, to post on servers or to redistribute to lists, requires prior specific permission and/or a fee. Request permissions from [permissions@acm.org](https://permissions.acm.org).

*MobiHoc '21, July 26–29, 2021, Shanghai, China*

© 2021 Copyright held by the owner/author(s). Publication rights licensed to ACM.

ACM ISBN 978-1-4503-8558-9/21/07...\$15.00

<https://doi.org/10.1145/3466772.3467035>

*Theory, Algorithmic Foundations, and Protocol Design for Mobile Networks and Mobile Computing (MobiHoc '21), July 26–29, 2021, Shanghai, China. ACM, New York, NY, USA, 10 pages. <https://doi.org/10.1145/3466772.3467035>*

## 1 INTRODUCTION

It is well known that mobile devices are now hungrier than ever for gigabit-per-second data rates [1]. Thanks to their promise of data rates orders of magnitude higher than sub-6 GHz technologies [2], millimeter wave (mmWave) communications lie at the foundation of 5th generation (5G) networks and beyond [3, 4]. Among others, one of the core challenges in mmWave networks is the severely increased path loss with respect to sub-6 GHz frequencies, which implies that highly-directional communications through beamforming are necessary to bring the transmission range back to acceptable levels [5]. As a consequence, the transmitter (TX) and the receiver (RX) need to coordinate to select the beam pair that yields the highest beamforming gain. For this reason, *beam management* in mmWave networks has attracted tremendous interest from the research community over the last years [6–9].

### Background and Motivation

Beam management is usually a complex procedure that involves several time-consuming steps. First, both the TX and the RX need to discover each other by finding the initial beamforming vectors that yield sufficient Signal-to-Noise-Ratio (SNR) to establish a link. This crucial procedure is usually called *initial access* (IA) [10, 11]. Once the mmWave link has been established, *beam tracking* is performed to keep the TX and RX beams aligned to avoid sudden drops in SNR. For both IA and beam tracking, the 3rd Generation Partnership Project (3GPP) NR standard for 5G communications utilizes synchronization signal blocks (SSBs), which are essentially pilot and synchronization sequences that are periodically transmitted by the TX in each of its  $N_{tx}$  beam directions. By listening on each of its  $M_{rx}$  beam directions, the RX is then able to compute the received power for each of the  $N_{tx} \cdot M_{rx}$  possible beam combinations, and thus make an informed decision on which beamforming vector to use. The complexity of these beam management techniques, also called exhaustive beam sweep (EBS), is thus quadratic in the number of beams. Figure 1(a) shows an example of EBS when  $N_{tx} = 4$  and  $M_{rx} = 4$  beams are used. A similar, multi-stage procedure is used for IEEE 802.11ad [12], where the beams are distributed in  $N_{tx} \leq 128$  sphere sectors, with beam widths as small as 3 degrees [13]. A beam sweep is performed by the TX to find the best sector, and, subsequently, intra-sector fine-tuning is used by the TX and RX to refine the selection [14].

One can intuitively see that pilot-based EBS is very inefficient. For example, in 3GPP NR it could take up to 164 milliseconds (ms) to complete an IA when 24 beams are used by both TX and RX [7]. Worse yet, although EBS procedures could be feasible in cellular networks, they may not be effective at all in mmWave ad hoc

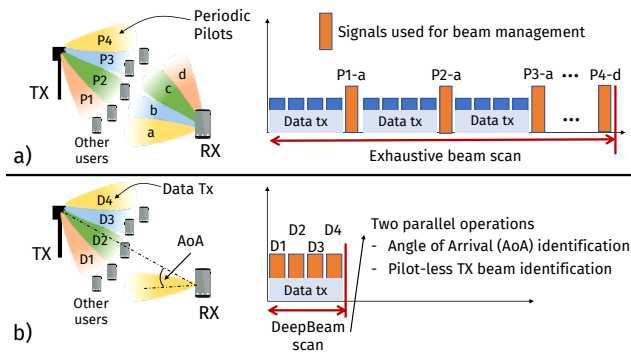


**Fig. 1: Traditional, pilot-based EBS (a) vs. DeepBeam (b).** In this example, with the EBS, the TX and RX scan 4 beams each, by transmitting pilots P1-P4 on different transmitter’s beams (TXBs), and by receiving with beams a-d, respectively, in specific time and frequency resources. With DeepBeam, the RX infers the Angle of Arrival (AoA) and the TXB by passively eavesdropping on data transmissions to other users in the network.

networks [15], where links are highly volatile and short in duration. For this reason, existing work – discussed in detail in Section 6 – has proposed several strategies to improve beam management [13, 16–28]. However, prior approaches still require coordination between the TX and RX, which reduces the effective channel utilization.

In this paper, we take a completely new direction: **we leverage a data-driven approach based on convolutional neural networks (CNNs) to achieve coordination-free beam management in mmWave networks.** Our core intuition – explained in details in Section 2.1 – is that different beams will impose different “impairments” to the waveform. These impairments will form a unique “signature” of the beam, which translates into a small-scale distortion of the emitted waveform. Therefore, a CNN can learn to recognize these unique patterns in the in-phase-quadrature (I/Q) representation of the waveform and thus ultimately distinguish among different beams. The key advantage of our approach is that the beam can be inferred by simply eavesdropping on ongoing transmissions between the TX and other RXs, without any explicit synchronization. We use CNNs instead of traditional machine learning (ML) approaches since they can learn complex features that may not be clearly separable in a low-dimensional space [29–31], while also meeting real-time constraints [32]. Moreover, CNNs allow DeepBeam to be independent from device and scenario through fine-tuning or cross-training techniques, as CNNs do not require any antenna- or waveform-specific feature extraction process [33].

## Novel Contributions

We summarize the core contributions of this paper below.

- We design *DeepBeam*, the first framework that leverages waveform-level deep learning to perform beam management in mmWave networks without requiring explicit coordination between the TX and RX (Section 2). Instead, we leverage *ongoing transmissions* between the TX to other receivers and infer through *waveform-level deep learning* (i) the AoA of the TXB; and (ii) the TXB itself. By using these two pieces of information, the RX can infer how to switch its beam toward the TX, and can inform the TX of which is the best beam to be used for communications with the RX, without the need for explicit pilots. Figure 1(b) summarizes at a very high level why our approach drastically decreases the time taken to

identify the best beams to be used for the ongoing mmWave links by doing away with pilot-based scanning thanks to deep learning;

- Our data-driven approach has been extensively validated with a massive mmWave data collection campaign (Section 4). We utilize a well-known experimental mmWave prototype by NI [34] to collect more than 4 TB of mmWave waveforms with (i) 4 phased array antennas at 60.48 GHz, (ii) 2 codebooks containing 24 one-dimensional beams (*i.e.*, azimuth only) and 12 two-dimensional beams (*i.e.*, azimuth and elevation); (iii) 3 receiver gains; (iv) 3 different AoAs; (v) multiple TX and RX locations. Furthermore, we also leverage two custom-designed mmWave software-defined radios based on (i) off-the-shelf Xilinx ZCU111 RFSoc-based evaluation boards; and (ii) transceiver boards with 4 fully-digital RF chains, operating in the unlicensed 57-64 GHz frequency band with 2 GHz bandwidth [35]. Moreover, we perform a latency analysis of the proposed approach through a field-programmable gate array (FPGA) implementation of our CNN (Section 3). Experimental results conclude that DeepBeam (i) **achieves accuracy of up to 96%, 84% and 77% with a 5-beam, 12-beam and 24-beam codebook, respectively (Section 5); (ii) reduces latency by up to 7x with respect to the 5G NR initial beam sweep** in a default configuration and with a 12-beam codebook. We also provide results that investigate how DeepBeam I/Q learning generalizes for training and testing over different phased array antennas and TX and RX locations, and investigate cross-training approaches.

- A major contribution of this paper is that **we release the experimental waveform dataset to the community, as well as the code used for training and testing our models**<sup>1</sup>. So far, machine learning research in the mmWave domain has been severely stymied from the lack of experimental datasets, with most of the current research conducted with data obtained through simulations [36] and ray-tracing [37–39]. With our paper, we will enable other researchers to replicate our results and benefit from the data.

## 2 THE DEEPBEAM SYSTEM

The DeepBeam system, shown in Figure 2, is a stand-alone module that can be plugged into the Physical (PHY) and Medium Access Control (MAC) layers of a generic mmWave protocol stack. In other words, it does not rely on any specific feature of, for example, 3GPP NR or IEEE 802.11ad/ay. DeepBeam can be implemented in software, or on FPGAs, to provide real-time learning with latency guarantees [40]. DeepBeam can be easily integrated with the PHY and MAC layers through two interfaces, as shown in Figure 2. The first is a trigger that activates DeepBeam when required by the protocol stack. The second is a producer/subscriber interface to which the wireless stack can subscribe to consume the information generated by DeepBeam at its own convenience. This data consists of a list of tuples with three elements, *i.e.*, the AoA and the TXB, both inferred through deep learning, and the associated Reference Signal Received Power (RSRP), a metric that can be used to evaluate the quality of a received signal [41].

The input of DeepBeam consists of the raw digital waveform obtained through the receiver Radio Frequency (RF) chain, *i.e.*, the in-phase and quadrature (I/Q) data sampled by the Analog to Digital

<sup>1</sup>Dataset: <http://hdl.handle.net/2047/D20409451>, repository: <https://github.com/wineslab/deepbeam>

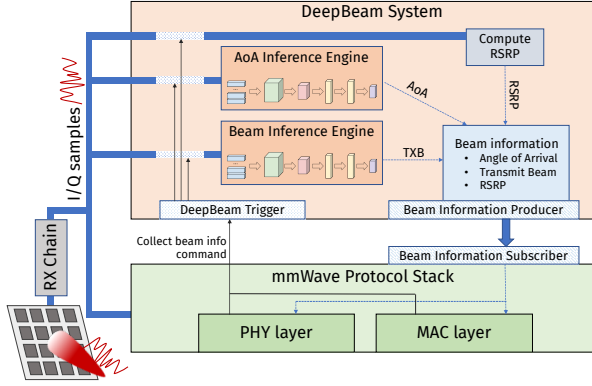


Fig. 2: DeepBeam Framework. The RX chain converts the analog waveform impinging the phased array into I/Q samples, which are processed by the PHY and MAC layers and by DeepBeam. In this, the I/Q samples are used to classify the TXB and AoA, and to estimate the RSRP. The mmWave protocol stack connects to DeepBeam through two interfaces, a trigger (to activate DeepBeam) and a data source, to obtain the TXB, AoA, and RSRP.

Converter (ADC), without any further processing (e.g., frequency offset tracking, equalization) from the PHY layer. This means that the module can be directly connected to the device RF chain, and that there is no need for synchronization between the transmitter and the receiver, as DeepBeam can handle the I/Q samples even before they are processed at the PHY layer. Therefore, a device equipped with DeepBeam can passively eavesdrop transmissions in a certain area, and collect statistics on the channel quality associated to the beams that a base station or access point uses to communicate with other users, eventually inferring what is the best beam pair to use for communications.

The two learning engines at the core of the DeepBeam module are based on CNNs, and use the I/Q samples to infer two key elements for beam management procedures, namely the TXB and AoA. These are usually obtained through a pilot-based beam sweep or inference at the transmitter and receiver [16, 18]. DeepBeam, instead, can perform the inference on any kind of over-the-air signal, thus speeding up beam management procedures, as we will discuss in Section 3. The AoA, as shown in Figure 3, corresponds to the angle with which the received signal impinges the antenna array of the receiver, either through the direct path between the transmitter and the receiver, when in Line-of-Sight (LOS), or through a reflected path, in Non-Line-of-Sight (NLOS). Thanks to this information, the RX can steer the receive beam toward this angular direction to experience the highest beamforming gain. This is shown, as an example, in Figure 3: the RX identifies that the AoA is AoA3, corresponding to, in this case,  $-45^\circ$ , and exploits this information to select the matching receive beam. Notice that traditional AoA detection methods either require multiple antennas and RF chains [42], or the sampling of the signal in multiple spatial location [43], while DeepBeam can operate directly on I/Q samples from a single RF chain. AoA detection (and RX-beam steering) can improve the performance of DeepBeam itself, as the RX would then be steering toward the TX and increase the classification accuracy thanks to a higher SNR.

DeepBeam also infers through deep learning which beam – from a certain codebook – is being used by the TX to transmit the waveform just sampled, as shown in Figure 3. Once the DeepBeam-equipped device has eavesdropped on enough ongoing transmissions, it can determine which is the best beam that the TX should

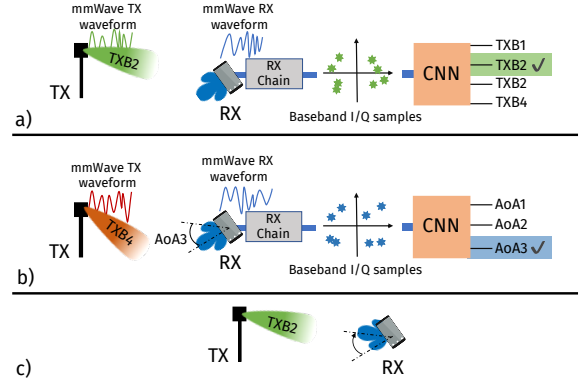


Fig. 3: TXB (a) and AoA (b) learning. In (a) and (b), a CNN processes the baseband I/Q samples to infer, respectively, the TXB used by the TX and the AoA. Then, (c) visually represents the final beam pair selection based on the inferred TXB and AoA.

use to communicate with it, for example, by ranking the inferred TXBs by the associated RSRP. Notice that several state-of-the-art techniques can also be integrated in DeepBeam to minimize the number of transmissions to observe. To this end, we point out that the pilot-less estimation that DeepBeam enables can be considered as a basis for further refinement of fast and efficient beam management schemes. The information regarding the best TXB can then be used in different ways during the beam management process. For example, in 3GPP NR the mobile device can infer with DeepBeam the best TXB, and then match it with the next synchronization signal block (SSB) in the same angular direction to perform initial access in the proper time and frequency resources. A detailed explanation of how DeepBeam can be used during the 3GPP NR initial access will be given in Section 3, together with an evaluation of the latency reduction obtained by using DeepBeam.

## 2.1 Beam and AoA Inference Engine

As mentioned earlier, DeepBeam leverages CNNs to perform real-time beam inference. We selected CNNs because of their demonstrated performance in addressing complex classification problems in the wireless domain, including modulation classification [30] and radio fingerprinting [44]. The versatility of CNNs is primarily owed to the fact that the filters in the convolutional (Conv) layers learn patterns in the I/Q constellation plane, regardless of where they occur in the waveform (*shift invariance*). This is necessary because there may be rotations in the received signal, induced by different channels, which would otherwise make the framework scenario-dependent. More formally, a Conv layer is trained to learn a series of  $F$  filters  $\mathbf{P}_f \in \mathbb{R}^{d \times w}$ ,  $1 \leq f \leq F$ , where  $d$  and  $w$  are the depth and width of the filter. An output  $\mathbf{O}^f \in \mathbb{R}^{n' \times m'}$  is produced from input  $\mathbf{I} \in \mathbb{R}^{n \times m}$  according to the following equation:

$$\mathbf{O}_{i,j}^f = \sum_{k=0}^{d-1} \sum_{\ell=0}^{w-1} \mathbf{P}_{d-k,w-\ell}^f \cdot \mathbf{I}_{i-k,j-\ell}, \quad 1 \leq i \leq n' \quad 1 \leq j \leq m', \quad (1)$$

where  $n' = 1 + \lfloor n + d - 2 \rfloor$  and  $m' = 1 + \lfloor m + w - 2 \rfloor$ . This ultimately helps distinguish waveforms far beyond what is possible with traditional dense networks, which were shown to not perform well in RF classification tasks [33]. Furthermore, as discussed earlier,

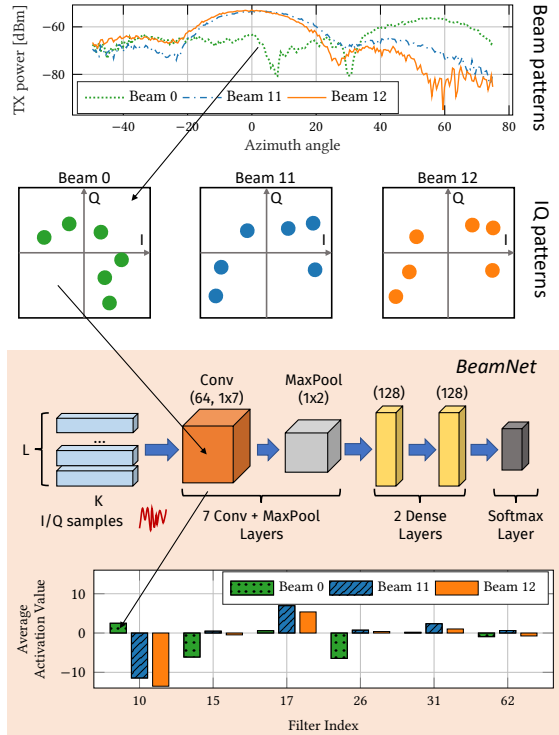


Fig. 4: Top: beam pattern for three different beams (0, 11, 12) of the 24-beams codebook (Sec. 4.1). Mid: examples of I/Q patterns for the different beams. Bottom: the baseline architecture of the *BeamNet* CNN and average activation value of the first convolutional layer for the same beams. The input of *BeamNet* is given by  $K$  I/Q samples grouped in  $L$  blocks.

CNNs are amenable to be implemented in FPGA and integrated in the baseband processing loop [32], and are easily fine-tunable [40].

We consider the *BeamNet* CNN architecture shown in Figure 4, which we call *baseline*. In the rest of the paper, if not explicitly mentioned otherwise, we will refer to the architecture above. Our baseline has been adapted from the architecture presented in [30], which has proven to be effective for RF classification tasks. *BeamNet* classifies input tensors of size  $(L, K, 2)$ , where  $L$  is the number of consecutive input blocks, each composed of  $K$  I/Q samples. By increasing the number of blocks, *BeamNet* will more likely recognize the I/Q patterns in the constellation. The input is further processed by 7 Conv layers, each followed by a maximum pooling (MaxPool) layer with filters of size  $1 \times 2$ , which ultimately reduce the output dimension of each Conv layer in half. Two dense layers follow the Conv + MaxPool layers, and finally a Softmax layer to obtain the probability of each beam or AoA.

We leverage a CNN since we want to learn short-size patterns in the I/Q constellation plane, which will ultimately distinguish different beamforming vectors [45]. To clearly explain this point, the top portion of Figure 4 shows the beam patterns (*i.e.*, the transmitted power as a function of the azimuth angle) for beams 0, 11, and 12 of the 24-beam codebook used in our experimental testbed described in Section 4.1. These patterns were obtained from the testbed vendor through measurements in an anechoic chamber. Figure 4 shows that beam 0 has a very different shape with respect to beams 11

and 12. In the middle portion of Figure 4, we also include example of different I/Q sequences for each of the beams.

The core idea is that the CNN filters will learn to distinguish these “imperfections” in the I/Q constellation plane. To further verify this is the case, we have investigated how the filters in the first convolutional layer of *BeamNet* react to the different beams. The bottom size of Figure 4 shows the average activation values (over the test set) for the filters in the first layer of *BeamNet* that have at least one positive value (six filters in total). We notice that beams 11/12 have a strong positive reaction to filter 17, which is also very similar in magnitude. Moreover, the strongest reaction for beam 0 happens for filter 10, where beams 11/12 have a strong negative activation value. This confirms that *BeamNet* is learning to distinguish beams by discriminating different patterns in the received I/Q waveform.

### 3 DEEPBEAM USE CASES

As mentioned earlier, DeepBeam is independent of the specific wireless protocol stack, since it relies on unprocessed I/Q samples and thus can be used for any beam management operation (*i.e.*, initial access, beam tracking, neighbor discovery). Nonetheless, to provide a concrete example of the effectiveness of DeepBeam, in the following paragraphs we will describe two use cases based on 5G protocol stacks, *i.e.*, the initial access for 3GPP NR and neighbor discovery in mmWave vehicular networks.

**Initial Access in 3GPP NR.** NR is a set of specifications for 5G cellular networks defined by the 3GPP Release 15 in 2018 and Release 16 in 2020. Its physical layer is based on Orthogonal Frequency Division Multiplexing (OFDM), with a flexible frame structure in which the symbol duration and subcarrier spacing can be adapted to match traffic requirements. Henceforth, we consider numerology 3 [46], with a symbol duration  $T_{\text{sym}} = 8.92 \mu\text{s}$ , and slots of 14 symbols with duration  $T_{\text{slot}} = 250 \mu\text{s}$ .

Beam management for the IA procedure in 3GPP NR involves four steps [7, 46]. In the first (*beam sweep*), the base station transmits directional Synchronization Signals (SSs) to cover all the TXBs of a certain codebook. Notably, each beam is swept with an SSB, which is a group of 4 OFDM symbols and 240 subcarriers in frequency. SSBs are interleaved to data transmissions in pre-defined time instants during bursts of 5 ms, as discussed in [47]. There can be at most  $N_{\text{SS}} = 64$  SSBs for each burst, and, if the sweep is not completed, the procedure resumes during the next burst. SS bursts are repeated with a periodicity  $T_{\text{SS}}$  that can be configured by the NR protocol stack (5 to 160 ms, with default 20 ms). During the SSB beam sweep, the User Equipment (UE) itself, if configured for directional reception, performs a directional scan, measuring the quality of each beam pair (second step, *beam measurement*). Then, the UE selects the beam to be used to perform initial access (third step, *beam decision*). During the next SSB in the selected direction, the UE acquires information on the time and frequency resources in which the base station will be in receive mode for the random access message using the same TXB (fourth step, *beam reporting*).

Let us consider an exhaustive beam sweep (EBS), with  $N_{\text{tx}}$  beams at the TX, and  $M_{\text{rx}}$  at the RX. Thus, the number of beams to be scanned is then  $N_{\text{tx}} M_{\text{rx}}$ . By adapting the analysis from [7] for an analog beamforming case, the time required to complete an EBS

(i.e., steps 1 and 2) with the 3GPP NR frame structure is

$$T_{\text{EBS}} = T_{\text{SS}} \left( \left\lceil \frac{N_{\text{Tx}} M_{\text{Rx}}}{N_{\text{SS}}} \right\rceil - 1 \right) + \hat{T}_{\text{EBS}}. \quad (2)$$

The first term of the sum in Equation 2 represents the time to scan the first  $(\lceil N_{\text{Tx}} M_{\text{Rx}} / N_{\text{SS}} \rceil - 1) N_{\text{SS}}$  SSBs, in bursts of  $N_{\text{SS}}$  SSBs. The remaining  $\hat{N}_{\text{SS}} = N_{\text{Tx}} M_{\text{Rx}} - (\lceil N_{\text{Tx}} M_{\text{Rx}} / N_{\text{SS}} \rceil - 1) N_{\text{SS}}$  will only occupy a portion  $\hat{T}_{\text{EBS}}$  of the 5 ms of the last SSB burst, i.e., following [47],

$$\hat{T}_{\text{EBS}} = \begin{cases} \frac{\hat{N}_{\text{SS}}}{2} T_{\text{slot}} - 2T_{\text{sym}} & \text{if } \hat{N}_{\text{SS}} \bmod 2 = 0 \\ \left\lceil \frac{\hat{N}_{\text{SS}}}{2} \right\rceil T_{\text{slot}} + 6T_{\text{sym}} & \text{otherwise.} \end{cases} \quad (3)$$

Thanks to the TXB and AoA inference, as highlighted in Figure 1, DeepBeam can skip the EBS by passively eavesdropping ongoing data and control transmissions between the TX and other users. As discussed in Section 2.1, DeepBeam needs to acquire  $\xi = K \cdot L$  I/Q samples to perform the classification task on the two inference engines. In 3GPP NR, each OFDM symbol is composed by  $S$  subcarriers, with  $24 \cdot 12 \leq S \leq 275 \cdot 12$  subcarriers for numerology 3 (i.e., at most 400 MHz of bandwidth for each carrier frequency). Assuming one I/Q sample for each subcarrier (i.e., without considering oversampling factors), DeepBeam needs to eavesdrop  $E = \lceil \xi / S \rceil$  OFDM symbols. Eventually, considering a TX that allocates  $J$  symbols to each user in its coverage area, with a round-robin scheduler, the time required for passive data collection on the  $N_{\text{Tx}}$  TXBs is

$$T_{\text{DB,d}} = \max\{J, E\} N_{\text{Tx}} T_{\text{sym}}. \quad (4)$$

In addition, the inference engines of DeepBeam require a certain processing time to perform the classification.<sup>2</sup> The end-to-end latency of the learning engine is  $T_{\text{DB,c,e2e}}$ , with the slowest layer providing results with a delay of  $T_{\text{DB,c,max}}$ . When implemented on FPGA, it is possible to exploit a pipeline effect, thus the network will classify  $N_{\text{Tx}}$  beams in  $T_{\text{DB,c,e2e}} + (N_{\text{Tx}} - 1)T_{\text{DB,c,max}}$ . Eventually, the overall delay (data collection and classification) of the DeepBeam engine for the 3GPP NR initial access is

$$T_{\text{DB}} = \max\{\max\{J, E\}T_{\text{sym}}, T_{\text{DB,c,max}}\}(N_{\text{Tx}} - 1) + \max\{J, E\}T_{\text{sym}} + T_{\text{DB,c,e2e}}. \quad (5)$$

**Latency Analysis with FPGA CNN Synthesis.** To understand whether DeepBeam can truly deliver an accuracy boost with respect to existing technologies, we have synthesized in FPGA an instance of the inference engine for the TXB classification. Specifically, we have considered a CNN with input size  $\xi = 512$  I/Q samples, a single convolutional layer with 16 filters, which yields an accuracy of 90% in a 5-beam classification problem (discussed in Section 5.1). For synthesis, we targeted a Xilinx Zynq-7000 with part number xc7z045ffg900-2, a commonly used for software-defined radio implementations [48, 49]. We used high-level synthesis (HLS) for our CNN design. HLS allows the conversion of a C++-level description of the CNN directly into hardware description language (HDL) code such as Verilog. Therefore, improved results could be achieved with different design and synthesis strategies that further optimize real-time operations and minimize latency. By pipelining portions of the design, we are able to obtain  $T_{\text{DB,c,e2e}} = 0.492$  ms, while  $T_{\text{DB,c,max}} = 0.34$  ms. The resource utilization of the CNN

<sup>2</sup>We consider the processing time negligible in the case of a traditional EBS, as a worst-case scenario for our comparison.

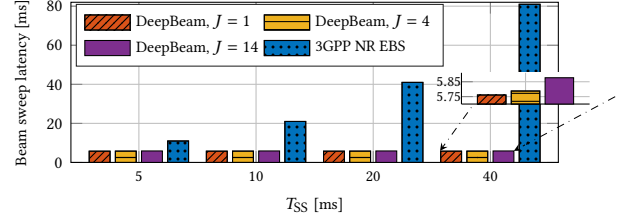


Fig. 5: Beam sweep latency, NR vs DeepBeam, for different values of the SS burst periodicity  $T_{\text{SS}}$  and of the number of contiguous symbols  $J$  allocated to each TXB by the base station scheduler.

design is below 5% – specifically, our design utilizes 32/1090 block RAMs, 28/900 DSP48E, 3719/437200 flip-flops and 2875/218600 look-up tables. Resource consumption can be further brought down by avoiding pipelining, to the detriment of latency.

Figure 5 reports  $T_{\text{EBS}}$  and  $T_{\text{DB}}$  for different values of  $T_{\text{SS}}$ . We assume numerology 3, a bandwidth of 400 MHz (i.e.,  $S = 3300$ ),  $N_{\text{Tx}} = N_{\text{Rx}} = 12$ , and different values of  $J$ , to represent various resource allocation policies of the NR base station. The results show how DeepBeam manages to decrease the beam sweep latency by a factor between 1.87 (for  $T_{\text{SS}} = 5$  ms) and 14.05 (for  $T_{\text{SS}} = 40$  ms). Notice that  $T_{\text{SS}} = 5$  ms represents a configuration where the overhead is rather high, as there is no interval between consecutive SSB bursts. In the default configuration with  $T_{\text{SS}} = 20$  ms, DeepBeam reduces the latency by up to 7.11 times.

**Neighbor Discovery in Vehicular Networks.** Beam tracking and neighbor discovery are even more challenging in vehicular scenarios [9], since the dynamics of the system reduce the coherence time and prevent from efficiently using pilot signals. Moreover, since neighboring vehicles may change the reciprocal position frequently, each node needs fresh information on the best beam selection before starting a communication with another peer.

Prior work on ad hoc mmWave communications relies on contextual information, custom hardware and/or signaling to perform beam management [50]. Conversely, Figure 6 illustrates how DeepBeam can be effective also in a mmWave vehicular/ad hoc scenario. In this example, four vehicles are proceeding on a two-lane street, transmitting and receiving data with the vehicle in the same lane. At the same time, the vehicles can use the DeepBeam inference engine

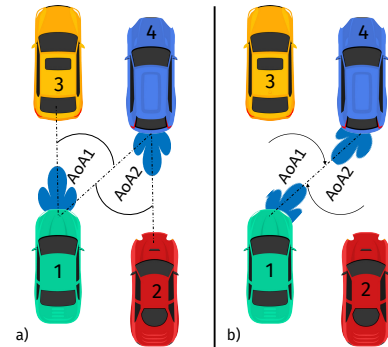


Fig. 6: DeepBeam in a vehicular ad hoc scenario. (a) Vehicle 1 is communicating with vehicle 3, vehicle 2 with vehicle 4. Using DeepBeam, vehicles 1 and 4 infer the reciprocal AoA by passively eavesdropping ongoing data transmissions. (b) Vehicles 1 and 4 can steer the beam toward each other when they need to exchange data.

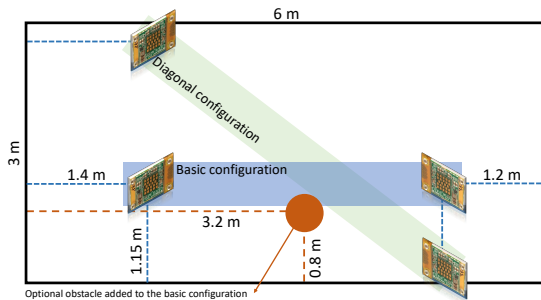


Fig. 7: Configuration of the room where the single-RF-chain dataset was collected, and position of the radios in the basic and diagonal configuration, and of the obstacle.

to classify the AoA of the waveform received from the transmissions of the vehicles in the other lane. For example, if IEEE 802.11ad is used, DeepBeam can perform data collection during the interframe intervals which are mandated by the standard specifications, e.g., the DCF Interframe Space (DIFS) and the Short Interframe Space (SIFS), which would allow the collection of 22880 and 5280 I/Q samples, respectively, over  $13 \mu\text{s}$  and  $3 \mu\text{s}$ . Moreover, as the data collection and classification can be performed while (in this example) vehicles 1 and 3 are communicating with each other, when vehicle 1 starts transmitting to vehicle 4, it is already aware of the TXB to use (i.e., that corresponding to the AoA classified by DeepBeam). This makes it possible to skip any beam sweep or coordination before the link establishment between vehicle 1 and vehicle 4. Once again, if considering IEEE 802.11ad, this could take up to  $225.4 \mu\text{s}$  for a codebook with 12 beams, according to [51].

## 4 EXPERIMENTAL SETUP AND DATASET

This section describes the two mmWave testbeds used to collect the waveform data (Sections 4.1 and 4.2), how our datasets are structured, and how the models were trained (Section 4.3).

### 4.1 Single-RF-chain Testbed

This testbed is based on the NI mmWave platform [34], with two software-defined transceivers implemented on FPGAs, mounted on PXIe chassis, and running a custom 802.11ad-like physical layer. Besides the FPGAs, each transceiver chassis includes an ADC and a Digital to Analog Converter (DAC), operating in baseband at 3.072 GS/s. The two nodes are equipped with 60 GHz radio frontends from SiBeam, which feature an up-conversion circuit, capable of bringing the signal to an RF carrier of 60.48 GHz, with an RF bandwidth of 1.76 GHz, and an analog phased array. The array (also shown in Figure 7) has 12 antenna elements for the TX chain, and 12 for the RX chain. Each element can be controlled with 4 phase settings (i.e., a rotation of  $0^\circ$ ,  $90^\circ$ ,  $180^\circ$ , or  $270^\circ$ ) to perform beam steering. By default, two codebooks are provided, with 24 beams in the azimuth plane, or 12 beams steered in the azimuth and elevation planes. The transmit power is 12 dBm, and it is possible to control the RX gain of the SiBeam boards. The physical layer in the two NI transceivers is based on IEEE 802.11ad, and generates (or receives) samples at a rate that matches that of the ADC/DAC. I/Q samples are aggregated in blocks of 2048 samples, and 150 blocks define a slot of  $100 \mu\text{s}$ . 100 slots are then grouped in a frame (10 ms), which constitutes the basic transmission unit.

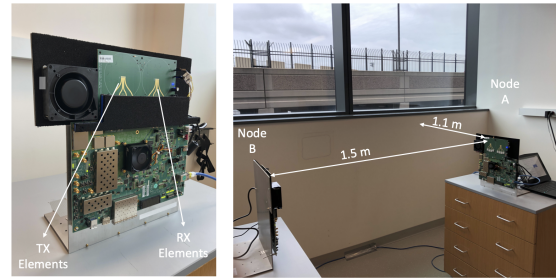


Fig. 8: Multi-RF-chain testbed setup.

For the data collection, the two mmWave nodes were positioned as in Figure 7, in a  $6 \times 3$  m room, with three different configurations. The first (i.e., *basic configuration*) features two arrays facing each other, at a distance of 3.4 m, and at 1.15 m from the side wall. They have the same position in the second setup (i.e., *obstacle configuration*), but an obstacle (i.e., a chair) is added in the space between the two antennas, without obstructing the LOS. In the third setting (i.e., *diagonal configuration*), the arrays face each other at a distance of 4.40 m, with the link crossing the room diagonally.

### 4.2 Multi-RF-chain Testbed

The second testbed features two fully-digital mmWave transceiver boards, shown in Figure 8, each based on an off-the-shelf Xilinx ZCU111 RFSoc-based evaluation board and a custom mezzanine board. This takes care of the RF up-conversion, and has two arrays (for the TX and the RX) with 4 patch antenna elements each [35]. With respect to the SiBeams radios, in this setup each antenna element is connected to an RF chain, with its own up-converters (with an output power of 12 dBm per channel), in the mezzanine board, and ADCs/DACs, on the Xilinx RFSoc. While the sampling rate of the ADCs/DACs is 3.93216 GS/s, with separate elements for the in-phase and quadrature components, the effective RF bandwidth is limited to 2 GHz by the up-converters and patch antennas. We operate the boards at a carrier frequency of 58 GHz. The two transceivers use a custom physical layer, based on OFDM, with a sampling rate that matches that of the ADCs/DAC, an oversampling factor of 4, and 256 subcarriers over a bandwidth of 1 GHz.

Differently from the single-RF-chain testbed, in which beamforming is performed in the analog domain by selecting one of the four phase shift available in each antenna elements, in the transceivers of this testbed the beamforming vector is applied digitally, i.e., the I/Q samples are multiplied by a vector of digital phase shifts (one for each of the 4 RF chains) before (after) the ADC (DAC) conversion. This enables the definition of more precise beam patterns, and more degrees of freedom with respect to the selection of the steering vector. The data collection for this pair of nodes was performed with the two transceivers facing each other, at a distance of 1.5 m, as shown in Figure 8.

### 4.3 Datasets Structure and Training Procedure

We collected more than 4 TB of raw I/Q samples to evaluate the performance of DeepBeam, using the single- and the multi-RF-chain testbeds. Table 1 summarizes the different configurations in which the data collection was performed. Notably, for the single-RF-chain testbed, we used four different SiBeam 60 GHz frontends, the three configurations described in Figure 7, and the two default TXB codebooks of the SiBeam phased arrays. For the AoA dataset, we

Classification target	TX Codebook	Testbed	Configuration	(TX, RX) antenna combinations
TXB	24-beams codebook	Single-RF-chain	Basic, with obstacle, diagonal	SiBeam (0, 1), (1, 0), (2, 1), (3, 1)
TXB	12-beams codebook	Single-RF-chain	Basic, with obstacle, diagonal	SiBeam (0, 1), (1, 0), (2, 1), (3, 1)
AoA	24-beams codebook	Single-RF-chain	Basic, with obstacle, diagonal	SiBeam (0, 1), (1, 0), (0, 2), (0, 3)
TXB	5-beams codebook	Multi-RF-chain	Multi-RF-chain basic	Node A, Node B

Table 1: Setups for the I/Q data collection. Dataset: <http://hdl.handle.net/2047/D20409451>, repository: <https://github.com/wineslab/deepbeam>

physically rotate the receive phased array by  $\theta \in \{-45^\circ, 0^\circ, 45^\circ\}$  with respect to the direction between the TX and RX. To collect data with low and high SNR (*i.e.*, in a range between -15 dB and 20 dB, according to the combination of TXB and gain), we consider three RX gain values for each configuration the single-RF-chain testbed, and three TX gain for the multi-RF-chain testbed. For both, the receiver’s beam (RXB) is always steered toward the boresight direction of the RX array. The raw I/Q data is collected in blocks of 2048 samples, for both the single-RF-chain and the multi-RF-chain testbed. For the first, we collected 150000 blocks for each combination of TXB and RX gain. For the second, we collected 50000 blocks for each combination of TXB and TX gain.

Our models were trained using the Adam optimizer [52] with a learning rate of  $l = 0.0001$ . Our training minimizes the prediction error over the training set through back-propagation, with categorical cross-entropy as loss function. We have implemented *BeamNet*, and the training/testing code in Keras, with TensorFlow as a backend. We used an NVIDIA DGX system equipped with 4 Tesla V100 GPUs. We trained our models for at least ten epochs, with batch size of 100. Our dataset was split into 60% training set and 40% testing set.

## 5 EXPERIMENTAL RESULTS

This section presents an extensive set of experimental results that validate the performance of DeepBeam. We first characterize the accuracy with different codebooks and different input size (Sec. 5.1). We then present insights on DeepBeam’s performance with different SNR levels and locations (Sec. 5.2). The third set of results explores how DeepBeam generalizes when trained on I/Q samples from a phased array antenna, and tested on another, and investigates cross-training solutions (Sec. 5.3). Finally, we discuss limitations and future extensions (Sec. 5.4).

### 5.1 Accuracy Results with Different Codebooks and Input Sizes

Figure 9 shows the confusion matrices (CMs) obtained by training *BeamNet* on the 12-beam and 24-beam codebooks, for two different values of the  $L$  input parameter, and  $K = 2048$ . The accuracy reaches above 80% and 77% in case of the 12-beam and 24-beam codebook, respectively. Figure 9 indicates that *BeamNet* is very accurate in predicting the beams far from the center. However, it also hints that the model gets confused when distinguishing among the central beams (11/12 and 5/6, respectively), as explained in Section 2.1.

To further elaborate on the impact of the codebook and CNN input size, we also tested DeepBeam on the dataset collected with the multi-RF-chain testbed. In particular, Figure 10a shows the accuracy as a function of the input size  $K$ . For this, we trained a smaller network than the baseline, with only one convolutional layer (with 12 filters of size 7) and no dense layer other than the

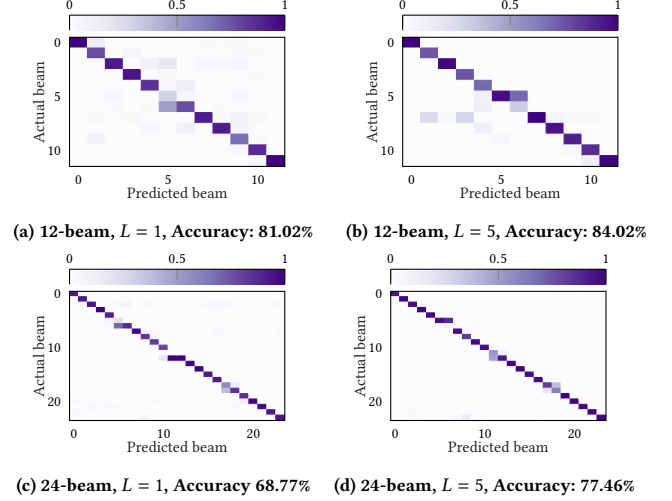


Fig. 9: Confusion matrices for 12- and 24-beam codebook, with TX antenna 0, RX antenna 1 and the basic configuration from the single-RF-chain testbed.

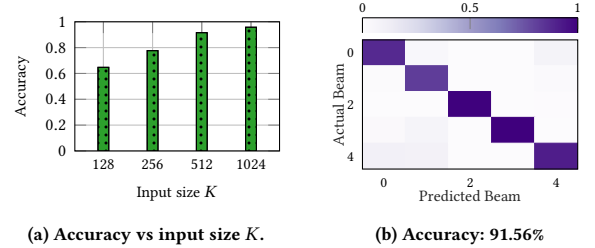


Fig. 10: Accuracy for a 5-beam codebook, using the multi-RF-chain testbed and a simplified CNN configuration.

softmax. Figure 10b shows the confusion matrix (CM) in the case of  $K = 512$ , where we achieve accuracy of 91.56%. We point out that we can achieve such high accuracy with a smaller model because in the multi-RF-chain testbed we apply beamforming vectors digitally, thus resulting in more precise beam patterns with respect to the single-RF-chain testbed. Nonetheless, this shows that DeepBeam can be applied on a heterogeneous set of devices.

### 5.2 Impact of the SNR and Location

The CMs of Figure 9 were obtained by mixing low, medium and high SNR waveforms. To get an insight on how the SNR impacts the accuracy of *BeamNet*, Figure 11 shows the CMs when low (*i.e.*, below 0 dB) and high (*i.e.*, above 10 dB) SNR waveforms are used to train and test the model. We only show the results for the 24-beam codebook due to space limitations. As experienced in much of existing work, Figure 11 definitely indicates that there is a strong correlation between the accuracy of the model and the SNR level of the received waveforms. The accuracy drops to 43% when low SNR samples are used, yet it goes up to 86% when *BeamNet* is trained with high SNR samples only.

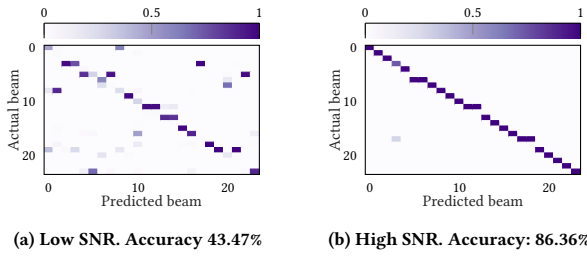


Fig. 11: Low and High SNR, 24-beam codebook,  $L = 1$ , with TX antenna 0, RX antenna 1 and the basic configuration from the single-RF-chain testbed.

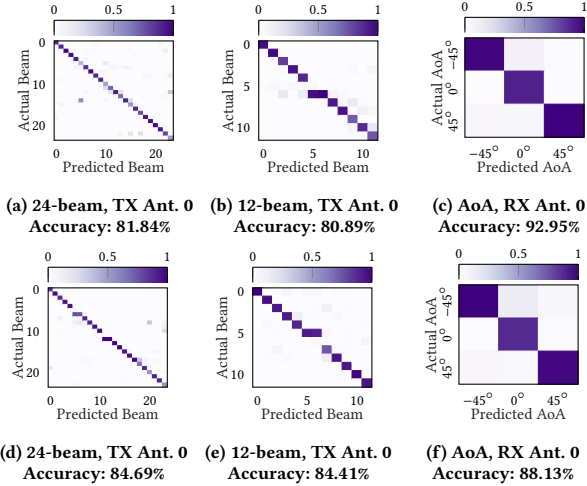


Fig. 12: Diagonal and Obstacle results with the single-RF-chain testbed.

To analyze the impact of the scenario on DeepBeam, we show the results obtained in the Diagonal and Obstacle configurations in Figure 12. Interestingly, we see that our CNN is flexible and robust to different conditions. In the case of 24-beam, we see a significant increase in accuracy with respect to the basic configuration, while the other accuracy results are in line with what experienced in the basic configuration.

### 5.3 Training and Testing on Different Devices

To understand whether the features learned by the CNN are related to the single antenna under consideration or generalize to multiple antennas, Figure 13 shows the accuracy results obtained by training on one antenna and testing on another (TOTA), with both codebooks and all four phased arrays, with different values of  $L$ . Therefore, the main diagonal shows the results for train and test with the same antenna (TTSA). The first insight revealed by Figure 13 is that the features learned by the CNN are a mixture of antenna-based and antenna-independent, since (i) the accuracy decreases when a CNN is tested on a dataset collected for a different antenna, but (ii) the accuracy does not plummet to random prediction.

Indeed, while the average TTSA accuracy is 83.08%, the average TOTA accuracy is 27.90%, which is more than 3x the random guess (1/12) in the 12-beam case when  $L = 1$ . Interestingly enough, we observe that while the average TTSA accuracy increase to 89.90% when  $L = 5$ , the average TOTA accuracy slightly decreases to 25.29%. This can be explained by the fact that a larger model will be more prone to overfitting. In this case, a smaller model will lead to less accuracy but more generalization. A similar effect is observed

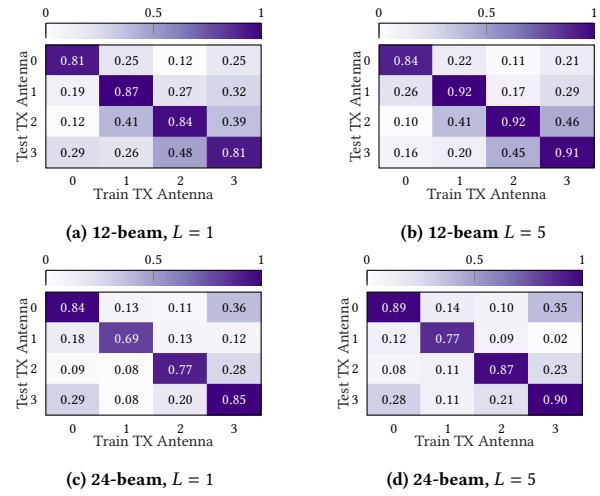


Fig. 13: Train One Test Another, 24-beam and 12-beam codebook with the single-RF-chain testbed.

in the 24-beam codebook, where the TTSA increases from 78.51% to 85.91% between  $L = 1$  and  $L = 5$ , but the TOTA slightly decreases from 16.97% to 15.35%.

Figure 14 shows the results obtained after training our CNN to detect the AoA of an incoming beam, for two different antennas. We also report the TOTA results in Figure 14(c). Figure 14 indicates that the CNN obtains a very high accuracy of more than 90%. As before, the TOTA results (57.57% in this case) show that the learned features are a mix of antenna-dependent and independent features.

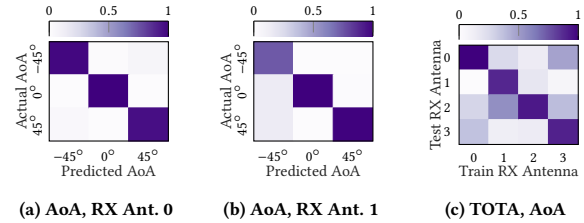


Fig. 14: AoA Results with the single-RF-chain testbed.

To further test the generalization capability of our CNN, we trained and tested it on a mixed dataset with waveforms coming from all 4 antennas. Figure 15 shows the obtained accuracy in all three learning problems when  $L = 1$ , and indicates that the CNN is very effective in generalizing to different antennas, increasing the accuracy of 124%, 191% and 44% in case of 24-beam, 12-beam and AoA with respect to the average TOTA accuracy experienced when trained with a single dataset. Similar results can be obtained when

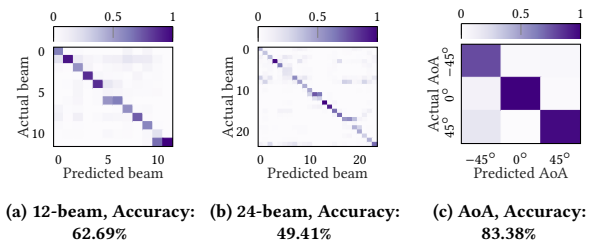


Fig. 15: Mixed train/test results with the single-RF-chain testbed.

training on one spatial configuration (e.g., basic, diagonal, obstacle) and testing on another.

#### 5.4 Discussion and Possible Extensions

The results presented in Section 5 highlight the efficacy of our CNN-based approach for the classification of the TXB and the AoA, demonstrating *for the first time* waveform learning approaches at mmWaves and confirming the intuition described in Sec. 2.1. In particular, DeepBeam is robust with respect different devices, antenna architectures, input sizes, SNR levels, and deployment scenarios. We believe that this opens new and exciting research directions, fostered also by the DeepBeam dataset, toward:

- The development of fine-tuning solution to improve the transferability of the learning process for directional transmissions in a wider range of scenarios. The results in Sec. 5.3 have shown how the proposed approach is robust with respect to training and testing on different devices, and how cross-training can help DeepBeam generalizing and achieving device independence. This work can be further extended by developing protocols and algorithms to deploy DeepBeam in new scenarios and with new radios, for which re-training or fine-tuning of the DeepBeam CNNs may be required [53]. In this regard, future work will develop automated data collection and labeling tools (e.g., with interaction between the device firmware and the DeepBeam framework) to enhance the training datasets for DeepBeam-equipped devices;
- The identification of the AoA with a model-free approach, on a single-RF-chain device, and without the need for multiple sampling in space and/or time (as, for example, in [43]). This paper has considered a subset of possible AoA values for the classification, but we plan to extend the dataset and evaluation to achieve a finer detection of the AoA.

## 6 RELATED WORK

Beam management is a key problem in mmWave networks, and has attracted significant interest [7, 13, 16–28, 54].

One of the earliest works in the field is due to [13], where Nitsche *et al.* utilize eavesdropping of legacy sub-6 bands to estimate the direction for pairing nodes. Va *et al.* propose a beam tracking algorithm in [16], which however assumes external AoA and Angle of Departure (AoD) estimators. The authors in [17, 18] propose beam training protocols that leverage hybrid analog-digital beamforming antennas to scan multiple spatial sectors simultaneously. Steinmetzer *et al.* [19] adapt compressive path tracking for sector selection in off-the-shelf IEEE 802.11ad devices, where the strength of received frames is used to sweep only through a subset of probing sectors. Loch *et al.* [20] track both movement and rotation of 60 GHz mobile devices with a zero-overhead mechanism, where part of the preamble of each packet is transmitted using a multi-lobe beam pattern. Zhou *et al.* [21] present a model-driven approach that performs a virtual scan based on a spatial channel profile built at the receiver, which however is bootstrapped using environmental information. Sur *et al.* [22] propose a beam sweeping algorithm with reduced complexity, thanks to a space-time analysis of the directional paths that reduces the number of directions to scan. Zhou *et al.* present in [54] a 3D beam sweeping along a “cross” around the central direction. Zhou *et al.* propose in [23] a beam tracking mechanism to address beam misalignment between Unmanned Aerial Vehicles

(UAVs). Ghasempour *et al.* [24] proposed a system leveraging channel sparsity and the knowledge of the beam codebook to construct a set of candidate beams for multi-stream beam steering. Aykin *et al.* [27] propose a multi-armed bandit framework for beam tracking based on ACK/NACK feedback, where reinforcement learning is used to select the appropriate beams and transmission rates. In [28], the authors propose a log-time peak finding algorithm to find the best beam in a three-dimensional space.

All the above work requires some sort of coordination with the TX, which in turn introduces overhead. Our approach in *DeepBeam*, instead, is *fully passive* and does not need any information exchange with the TX. Regarding passive beam tracking, Haider *et al.* proposed in [25] *LiSteer*, a mechanism using external light-emitting diodes (LEDs) located on the wireless Access Point (AP) to track the user’s movement. However, the mechanism requires additional equipment and may not work in many circumstances (*i.e.*, visible light is present, mobile device inside the pocket, and so on). Moreover, it requires traditional beam sweeping at the AP side. In the paper, we demonstrated that our methodology is *standard-agnostic* and *antenna-agnostic* and can be utilized at both TX and RX side.

The application of deep learning to improve the performance of wireless communications has seen a steadfast rise in the research community over the last few years. Specifically, deep learning is being used to address challenging problems such as modulation recognition, radio fingerprinting, and many others [29, 30, 55, 56]. The interest in this technique comes from its versatility in addressing a wide variety of wireless classification problems where an explicit mathematical model is cumbersome to obtain (*e.g.*, because of the phenomenon itself or due to the scale of the classification problem). System aspects of deep learning in wireless have been also recently investigated in [32, 40], which have proven its applicability to address real-time classification problems. On the other hand, machine learning in the mmWave domain is still at its infancy, also due to the current lack of large-scale experimental databases. Existing relevant studies in the mmWave domain use either simulations or ray tracing, which may not entirely capture the complexity of real-life propagation scenarios at mmWave spectrum bands, and do not consider deep learning on I/Q samples [9, 36, 37, 39, 57]. To the best of our knowledge, this paper is the first to utilize experimental real-world data to address a practical deep learning problem in the mmWave domain.

## 7 CONCLUSIONS

In this paper, we have presented *DeepBeam*, a framework for beam management in mmWave networks that eliminates the need of beam sweeping by inferring through deep learning the direction and the AoA of the transmitter beam. We have conducted an extensive experimental data collection campaign with two software-defined radio testbeds, and by using multiple antennas, codebooks, gains and locations. We have also implemented our learning models on FPGA to evaluate the latency performance. Results show that *DeepBeam* (i) achieves accuracy of up to 96%, 84% and 77% with a 5-beam, 12-beam and 24-beam codebook, respectively; (ii) reduces latency by up to 7x with respect to the 5G NR initial beam sweep in a default configuration and with a 12-beam codebook. To allow repeatability, we also share our waveform datasets and the full *DeepBeam* code repository with the community.

## ACKNOWLEDGEMENTS

This work was supported in part by the US National Science Foundation under Grants CNS-1923789 and CCF-1937500. The authors would like to thank the anonymous reviewers for their insightful comments, and Yin Sun for shepherding the paper.

## REFERENCES

- [1] Ericsson Incorporated, "Ericsson Mobility Report," June 2020.
- [2] S. Akoum, O. El Ayach, and R. W. Heath, "Coverage and Capacity in mmWave Cellular Systems," in *Proc. of IEEE ASILOMAR*, pp. 688–692, 2012.
- [3] S. Rangan, T. S. Rappaport, and E. Erkip, "Millimeter-Wave Cellular Wireless Networks: Potentials and Challenges," *Proc. IEEE*, vol. 102, pp. 366–385, Mar 2014.
- [4] M. Giordani, M. Polese, M. Mezzavilla, S. Rangan, and M. Zorzi, "Toward 6G Networks: Use Cases and Technologies," *IEEE Commun. Mag.*, vol. 58, pp. 55–61, Mar 2020.
- [5] S. Dutta, C. N. Barati, D. Ramirez, A. Dhananjay, J. F. Buckwalter, and S. Rangan, "A Case for Digital Beamforming at mmWave," *IEEE Trans. Wireless Commun.*, vol. 19, pp. 756–770, Feb 2020.
- [6] L. Wei, Q. Li, and G. Wu, "Exhaustive, Iterative and Hybrid Initial Access Techniques in mmWave Communications," in *Proc. of IEEE WCNC*, 2017.
- [7] M. Giordani, M. Polese, A. Roy, D. Castor, and M. Zorzi, "A Tutorial on Beam Management for 3GPP NR at mmWave Frequencies," *IEEE Commun. Surveys Tuts.*, vol. 21, pp. 173–196, First Quarter 2019.
- [8] Y. Li, J. G. Andrews, F. Baccelli, T. D. Novlan, and C. J. Zhang, "Design and Analysis of Initial Access in Millimeter Wave Cellular Networks," *IEEE Trans. Wireless Commun.*, vol. 16, no. 10, pp. 6409–6425, 2017.
- [9] A. Asadi, S. Müller, G. H. Sim, A. Klein, and M. Hollick, "FML: Fast Machine Learning for 5G mmWave Vehicular Communications," in *Proc. of IEEE INFOCOM*, 2018.
- [10] M. Giordani, M. Mezzavilla, and M. Zorzi, "Initial Access in 5G mmWave Cellular Networks," *IEEE Commun. Mag.*, vol. 54, no. 11, pp. 40–47, 2016.
- [11] C. N. Barati, S. A. Hosseini, M. Mezzavilla, T. Korakis, S. S. Panwar, S. Rangan, and M. Zorzi, "Initial Access in Millimeter Wave Cellular Systems," *IEEE Trans. Wireless Commun.*, vol. 15, no. 12, pp. 7926–7940, 2016.
- [12] "IEEE Standard for Information Technology," *IEEE Std 802.11ad-2012 (Amendment to IEEE Std 802.11-2012, as amended by IEEE Std 802.11ae-2012 and IEEE Std 802.11aa-2012)*, pp. 1–628, 2012.
- [13] T. Nitsche, A. B. Flores, E. W. Knightly, and J. Widmer, "Steering With Eyes Closed: Mm-wave Beam Steering Without In-band Measurement," in *Proc. of IEEE INFOCOM*, 2015.
- [14] T. Nitsche, C. Cordeiro, A. B. Flores, E. W. Knightly, E. Perahia, and J. C. Widmer, "IEEE 802.11 ad: Directional 60 GHz Communication for Multi-Gigabit-per-second Wi-Fi," *IEEE Commun. Mag.*, vol. 52, no. 12, pp. 132–141, 2014.
- [15] A. Zhou, T. Wei, X. Zhang, and H. Ma, "FastND: Accelerating Directional Neighbor Discovery for 60-GHz Millimeter-wave Wireless Networks," *IEEE/ACM Trans. Netw.*, vol. 26, no. 5, pp. 2282–2295, 2018.
- [16] V. Va, H. Vikalo, and R. W. Heath, "Beam Tracking for Mobile Millimeter Wave Communication Systems," in *Proc. of the IEEE GlobSIP*, pp. 743–747, 2016.
- [17] D. De Donno, J. Palacios, and J. Widmer, "Millimeter-Wave Beam Training Acceleration Through Low-Complexity Hybrid Transceivers," *IEEE Trans. Wireless Commun.*, vol. 16, no. 6, pp. 3646–3660, 2017.
- [18] J. Palacios, D. De Donno, and J. Widmer, "Tracking Mm-Wave Channel Dynamics: Fast Beam Training Strategies Under Mobility," in *Proc. of IEEE INFOCOM*, 2017.
- [19] D. Steinmetzer, D. Wegemer, M. Schulz, J. Widmer, and M. Hollick, "Compressive Millimeter-Wave Sector Selection in Off-the-Shelf IEEE 802.11ad Devices," in *Proc. ACM CoNEXT'17*, p. 414–425, 2017.
- [20] A. Loch, H. Assasa, J. Palacios, J. Widmer, H. Suys, and B. Debaillie, "Zero Overhead Device Tracking in 60 GHz Wireless Networks Using Multi-Lobe Beam Patterns," in *Proc. ACM CoNEXT'17*, p. 224–237, 2017.
- [21] A. Zhou, X. Zhang, and H. Ma, "Beam-forecast: Facilitating Mobile 60 GHz Networks via Model-driven Beam Steering," in *Proc. of IEEE INFOCOM*, 2017.
- [22] S. Sur, I. Pefkianakis, X. Zhang, and K.-H. Kim, "Towards Scalable and Ubiquitous Millimeter-wave Wireless Networks," in *Proc. of ACM MobiCom*, 2018.
- [23] P. Zhou, X. Fang, Y. Fang, R. He, Y. Long, and G. Huang, "Beam Management and Self-healing for MmWave UAV mesh networks," *IEEE Trans. Veh. Technol.*, vol. 68, no. 2, pp. 1718–1732, 2018.
- [24] Y. Ghasempour, M. K. Haider, C. Cordeiro, D. Koutsonikolas, and E. Knightly, "Multi-Stream Beam-Training for MmWave MIMO Networks," in *Proc. of ACM MobiCom*, (New Delhi, India), p. 225–239, 2018.
- [25] M. K. Haider, Y. Ghasempour, D. Koutsonikolas, and E. W. Knightly, "LiSteer: mmWave Beam Acquisition and Steering by Tracking Indicator LEDs on Wireless APs," in *Proc. of ACM MobiCom*, pp. 273–288, 2018.
- [26] L. Yang and W. Zhang, "Beam Tracking and Optimization for UAV Communications," *IEEE Trans. Wireless Commun.*, vol. 18, no. 11, pp. 5367–5379, 2019.
- [27] I. Aykin, B. Akgun, M. Feng, and M. Krunz, "MAMBA: A Multi-armed Bandit Framework for Beam Tracking in Millimeter-wave Systems," *Proc. of IEEE INFOCOM*, 2020.
- [28] I. Aykin and M. Krunz, "Efficient Beam Sweeping Algorithms and Initial Access Protocols for Millimeter-wave Networks," *IEEE Trans. Wireless Commun.*, vol. 19, no. 4, pp. 2504–2514, 2020.
- [29] T. J. O'Shea and J. Hoydis, "An Introduction to Deep Learning for the Physical Layer," *IEEE Trans. Cogn. Commun. Netw.*, vol. 3, no. 4, pp. 563–575, 2017.
- [30] T. J. O'Shea, T. Roy, and T. C. Clancy, "Over-the-Air Deep Learning Based Radio Signal Classification," *IEEE J. Sel. Topics Signal Process.*, vol. 12, pp. 168–179, Feb 2018.
- [31] T. Jian, B. C. Rendon, E. Ojuba, N. Soltani, Z. Wang, K. Sankhe, A. Gritsenko, J. Dy, K. Chowdhury, and S. Ioannidis, "Deep Learning for RF Fingerprinting: A Massive Experimental Study," *IEEE Internet Things Mag.*, vol. 3, no. 1, pp. 50–57, 2020.
- [32] F. Restuccia and T. Melodia, "Big Data Goes Small: Real-Time Spectrum-Driven Embedded Wireless Networking Through Deep Learning in the RF Loop," *Proc. of IEEE INFOCOM*, 2019.
- [33] F. Restuccia and T. Melodia, "PolymoRF: Polymorphic Wireless Receivers Through Physical-Layer Deep Learning," *Proc. of ACM MobiHoc*, 2020.
- [34] NI, "Introduction to the NI mmWave Transceiver System." White Paper, 2019.
- [35] J. Haarla, V. Semkin, K. Zheng, A. Dhananjay, M. Mezzavilla, J. Ala-Laurinaho, and V. Viikari, "Characterizing 60 GHz Patch Antenna Segments for Fully Digital Transceiver," in *Proc. of EuCAP*, March 2020.
- [36] P. Zhou, X. Fang, X. Wang, Y. Long, R. He, and X. Han, "Deep Learning-based Beam Management and Interference Coordination in dense mmWave networks," *IEEE Trans. Veh. Technol.*, vol. 68, no. 1, pp. 592–603, 2018.
- [37] A. Alkhateeb, S. Alex, P. Varkey, Y. Li, Q. Qu, and D. Tujkovic, "Deep Learning Coordinated Beamforming for Highly-mobile Millimeter Wave Systems," *IEEE Access*, vol. 6, pp. 37328–37348, 2018.
- [38] A. Alkhateeb, "DeepMIMO: A Generic Deep Learning Dataset for Millimeter Wave and Massive MIMO Applications," in *Proc. of ITA*, Feb. 2019.
- [39] Y. Wang, M. Narasimha, and R. W. Heath, "MmWave Beam Prediction with Situational Awareness: A Machine Learning Approach," in *Proc. of IEEE SPAWC*, 2018.
- [40] F. Restuccia and T. Melodia, "DeepWiERL: Bringing Deep Reinforcement Learning to the Internet of Self-Adaptive Things," *Proc. of IEEE INFOCOM*, 2020.
- [41] 3GPP, "NR - Physical Layer Measurements - Rel. 15." TR 38.215, 2017.
- [42] O. A. Oumar, M. F. Siyau, and T. P. Sattar, "Comparison between MUSIC and ESPRIT direction of arrival estimation algorithms for wireless communication systems," in *Proc. of the First International Conference on Future Generation Communication Technologies*, pp. 99–103, Dec 2012.
- [43] T. Wei, A. Zhou, and X. Zhang, "Facilitating Robust 60 GHz Network Deployment By Sensing Ambient Reflectors," in *Proc. of USENIX NSDI*, pp. 213–226, Mar. 2017.
- [44] S. Riyaz, K. Sankhe, S. Ioannidis, and K. Chowdhury, "Deep Learning Convolutional Neural Networks for Radio Identification," *IEEE Commun. Mag.*, vol. 56, no. 9, pp. 146–152, 2018.
- [45] F. Restuccia and T. Melodia, "Deep Learning at the Physical Layer: System Challenges and Applications to 5G and Beyond," *IEEE Commun. Mag.*, vol. 58, no. 10, pp. 58–64, 2020.
- [46] 3GPP, "NR and NG-RAN Overall Description - Rel. 15." TS 38.300, 2018.
- [47] 3GPP, "Discussion on Remaining Issues of SS Block and SS Burst Set." Motorola Mobility, Lenovo - Tdoc R1-1714212, 2017.
- [48] J. Xianjun, L. Wei, and M. Michael, "open-source ieee802.11/wi-fi baseband chip/fpga design," 2019.
- [49] Analog Devices Inc., "AD-FMCOMMS2-EBZ User Guide." <https://wiki.analog.com/resources/eval/user-guides/ad-fmcomms2-ebz>, 2018.
- [50] N. González-Prelcic, R. Méndez-Rial, and R. W. Heath, "Radar Aided Beam Alignment in MmWave V2I Communications Supporting Antenna Diversity," in *Proc. of ITA*, Jan 2016.
- [51] A. Patra, L. Simić, and M. Petrova, "Design and Experimental Evaluation of a 2.4 GHz-AoA-enhanced Beamsteering Algorithm for IEEE 802.11ad mm-wave WLANs," in *Proc. of IEEE WoWMoM*, June 2017.
- [52] D. P. Kingma and J. Ba, "Adam: A Method for Stochastic Optimization," *arXiv preprint arXiv:1412.6980*, 2014.
- [53] N. Tajbakhsh, J. Y. Shin, S. R. Gurudu, R. T. Hurst, C. B. Kendall, M. B. Gotway, and J. Liang, "Convolutional neural networks for medical image analysis: Full training or fine tuning?," *IEEE Trans. Med. Imag.*, vol. 35, pp. 1299–1312, May 2016.
- [54] A. Zhou, L. Wu, S. Xu, H. Ma, T. Wei, and X. Zhang, "Following the Shadow: Agile 3-D Beam-steering for 60 GHz Wireless Networks," in *Proc. IEEE INFOCOM*, 2018.
- [55] J. Jagannath, N. Polosky, A. Jagannath, F. Restuccia, and T. Melodia, "Machine Learning for Wireless Communications in the Internet of Things: A Comprehensive Survey," *Ad Hoc Networks (Elsevier)*, vol. 93, p. 101913, 2019.
- [56] Q. Mao, F. Hu, and Q. Hao, "Deep Learning for Intelligent Wireless Networks: A Comprehensive Survey," *IEEE Commun. Surveys Tuts.*, Fourth quarter 2018.
- [57] G. H. Sim, S. Klos, A. Asadi, A. Klein, and M. Hollick, "An Online Context-Aware Machine Learning Algorithm for 5G mmWave Vehicular Communications," *IEEE/ACM Trans. Netw.*, vol. 26, no. 6, pp. 2487–2500, 2018.